energy&fuels

Article

pubs.acs.org/EF

Inorganic Phase Transformation in *Miscanthus* Ash

Judit Kaknics,*[,†] Françoise Defoort,[‡] and Jacques Poirier[†]

[†]Conditions Extrêmes et Matériaux: Haute Température et Irradiation (CEMHTI), UPR3079 CNRS, 1D Avenue de la Recherche Scientifique, 45071 Orléans Cedex 2, France

[‡]CEA/DRT/LITEN/DTBH/LTB, 17 Rue des Martyrs, 38054 Grenoble Cedex 9, France

ABSTRACT: The aim of this work is to describe the inorganic phase transformation of *Miscanthus* × *giganteus* ash at a high temperature taking into account the effect of oxidizing/reducing atmospheres and different harvest periods. A double approach was used: thermodynamic calculations and experimental validation in laboratory devices. The samples were characterized by scanning electron microscopy−energy-dispersive X-ray spectroscopy (SEM−EDX) and X-ray diffraction (XRD). Below 800 °C, the inorganics are mainly present as salts [KCl, K_2SO_4, and $Ca_3(PO_4)_2$], carbonates ($CaCO_3$), and SiO_2, while at higher temperatures (>900 °C), the solid phase is enriched in $CaSiO_3$ and $Ca_3(PO_4)_2$. The ash starts to melt around 750 °C, and the liquid phase is composed of SiO_2, K_2O, and CaO. The main difference between oxidizing and reducing atmospheres is the form of sulfur. In an oxidizing atmosphere, K_2SO_4 is formed, while in a reducing atmosphere, only traces of organically attached S were detected by SEM−EDX and most of the S has volatilized. The thermodynamic calculations were performed using the software package FactSage 6.4 with two different oxide databases: FToxid and GToxid. GToxid database predicts a higher solidus temperature (T_s > 900 °C) but greater liquid/solid ratio than FToxid (T_s ≈ 740 °C). Both databases predict the formation of K silicates or K−Ca (Mg) silicates below 800 °C, while the main solid phase observed by XRD was SiO_2. Reasons are linked to uncertainties in the initial mass balance of ashes, database uncertainties, and limitations of the diffusion and chemical reaction of elements. The composition of the liquid phase is well-described in both databases, although GToxid gives somewhat closer results to the SEM−EDX analysis with the incorporation of Ca and Mg into the liquid phase.

1. INTRODUCTION

The demand for energy diversification and the European Union (EU) objectives highlight the interest in new biomass sources and technology development. In thermal processes, the inorganic composition of biomass is crucial because inorganics can increase the product yield via their catalytic effect;[1−3] however, volatile compounds, such as alkali metals and chlorine, can damage the pipeline system by corrosion, and low-melting-point alkali silicates in the bottom ash can lead to slagging, fouling, or agglomeration. This study focuses on an herbaceous energy crop, *Miscanthus* × *giganteus*, which has been successfully cultivated in Europe and the U.S. for the last 30 years. Although an autumn harvest would give 30−60% higher yield, *Miscanthus* is usually harvested from February to April because its quality improves with a delayed harvest. The ash content decreases over the winter as a result of the leaf loss and the mineral wash out. Its moisture content declines as well as a result of the drying effect of the wind.[4]

The main inorganics in lignocellulosic biomass are K, Na, Ca, Mg, Si, P, S, and Cl, and in a small amount, Al, Fe, and Mn can be found as well. The chemical form of these elements is of great importance because it will affect the quantity of the liquid phase and the composition of the fly ash and bottom ash. Inorganics are present in different forms in the plant to serve different functions, such as the structural support and the transport of ions and organic molecules.[5−7] Minerals can also derive from an external source, from soil traces or pollution during the harvest and processing.[8] It is important to be aware of the presence of the external minerals because they can modify the ash behavior; e.g., the aluminum silicates from the soil can bind potassium and alter the ash-melting tendencies.[8,9]

Several methods exist to evaluate the risks related to ash melting during combustion or gasification. Fuel ash characterization methods are based on the change of certain physical parameters with the appearance of the liquid phase upon heating an ash sample,[10] but such characterization methods, for example, the most commonly used ash fusibility test (AFT), have many problems and are poorly reproducible.[11] For example, Dupont et al. observed a difference of 500 °C when performing the AFT for the same biomass in different laboratories.[12] The ash behavior predictive indices compare the proportion of easily volatile (N, S, and Cl), melt-forming (K and Na), and stable (Ca and Mg) elements.[13−18] These indices are not universal, because they were originally developed for coal and later adapted to biomass for fluidized-bed applications; hence, they may not be relevant to all cases.

The laboratory and pilot experiments are time-consuming and expensive; moreover, because of the numerous elements, the characterization of biomass ashes is challenging. Therefore, many studies tried to use a "cheaper" method, such as thermodynamic equilibrium calculations, to predict the ash behavior during biomass thermal processes.[19−27] In the case of thermodynamic calculations, the appropriate choice of databases and solution phases is crucial because they can alter the composition of the gaseous, liquid, and solid phases at a high temperature. The results must be interpreted with care because the calculations regarding the molten biomass ash have certain limits: the liquidus temperature of the ash can have a 200 °C

Received: May 28, 2015
Revised: September 7, 2015
Published: September 7, 2015

DOI: 10.1021/acs.energyfuels.5b01189
Energy Fuels 2015, 29, 6433−6442

difference compared to the experimental results.[19,20] This uncertainty is first due to an incomplete description of the thermodynamic database: not all of the binary and ternary systems have been evaluated and optimized, and these subsystems are considered to be ideal solutions or have been approximated.[28] In lignocellulosic biomass ashes, the molten phase is mainly composed of K_2O-SiO_2-CaO, but for the moment, no accurate data are available regarding this ternary system. Since the work of Morey et al. in 1930,[29] this ternary-phase diagram $K_2O-CaO-SiO_2$ has not been completed. Another drawback is that the software calculates the thermodynamic equilibrium considering infinite reaction time, while the residence time in some industrial processes is too short (a few seconds or minutes).[21,30] Solid–solid or solid–liquid phase reactions are in general slower than solid–gas, liquid–gas, or gas–gas phase reactions, but the equilibrium is expected to be reached fast enough in most of the cases because of the high temperature involved in the process (>800 °C). Moreover, the presence and decomposition temperature of different organic structures (cellulose, hemicellulose, and lignin) is not considered in the calculations. The chemical fractionation analysis of biomasses and biomass ashes showed that alkali earth metals are bound to the organic structure;[1,30] hence, the chemical reaction between Ca, Mg, and Si is limited at low temperatures.

Although many studies reported on the inorganic composition of different biomass samples and ashes after the thermal processes,[11,31,32] only few of them gave a detailed description of phase transformations as a function of the temperature[11,32−34] and none of them described the evolution of solid and liquid phases in *Miscanthus* ashes. In a former study, the interaction between molten *Miscanthus* ashes and different bed materials were investigated to describe the agglomeration characteristics in fluidized-bed applications.[35] This work completes the former results with a detailed study of inorganic phase transformations in *Miscanthus* ash in the temperature range of 400–1400 °C. This work has two main objectives: first, to describe the ash transformation focusing on the solid and liquid phase formation under equilibrium conditions in different atmospheres and with different harvest periods, and second, to evaluate the accuracy of different thermodynamic databases for biomasses rich in K and Si.

2. MATERIALS AND METHODS

2.1. Fuel. The *Miscanthus* (species *Miscanthus* × *giganteus*), further referred to as LM1, used in this study was harvested in April 2011 in La Ferté Chevresis, France. Table 1 shows the ultimate analysis of LM1 and the ash composition at 815 °C. To evaluate the impact of the autumn harvest, 5 kg of *Miscanthus* (called "LM2") was collected from the same plot of land. The collected *Miscanthus* was defoliated, and only the stems were compared to see the difference in the inorganic evolution over the year.

2.2. Ash Preparation. Because of the low ash content of *Miscanthus* (2.1%), a very large quantity of feedstock is necessary to obtain a sufficient quantity (several tens of grams) for the study. No facility large enough was available at the laboratory to fabricate such an amount in an oxidizing (air) or a reducing atmosphere (air default as in air gasification) in the range of 400 and 1400 °C. Therefore, a startup batch of a large quantity of ash was prepared at 400 °C, a temperature low enough to allow for accumulation of the inorganics with keeping the volatilization of alkali metals and modification of inorganic phases at the lowest possible level as requested by Osman et al.[36] already in 1983 and Bryers et al.[6] A lower temperature would have resulted in an elevated amount of char, which would have limited the characterization of the samples.

Table 1. Analysis of *Miscanthus* × *giganteus* (April 2011, La Ferté Chevresis, France) called "LM1"

Miscanthus (LM1)			
moisture content (wt %)	15.1		
carbon (wt %, dry)[a]	48.6		
oxygen (wt %, dry)[b]	43		
hydrogen (wt %, dry)[a]	5.8		
nitrogen (wt %, dry)[a]	<0.3		
sulfur (mg/kg, dry)[c]	1669		
chlorine (mg/kg, dry)[c]	1002		
ash content at 815 °C (wt %, dry)	2.1		
ash composition at 815 °C (wt %)[d]			
oxide (wt %)		element (wt %)	
SiO_2	66.0	Si	31.0
K_2O	14.1	K	11.7
CaO	10.4	Ca	7.4
MgO	2.5	Mg	1.5
Na_2O	1.1	Na	0.8
P_2O_5	1.6	P	0.7
SO_3	1.5	S	0.6
Al_2O_3	1.0	Al	0.5
Fe_2O_3	1.1	Fe	0.8
TiO_2	<0.1	Ti	<0.06
MnO_2	0.3	Mn	0.2
		O	46.3

[a]Detected by a CHN microanalyzer. [b]Calculated. [c]Detected by ion chromatography. [d]Detected by inductively coupled plasma–mass spectrometry (ICP–MS).

LM1 and LM2 ash samples were prepared the following way: the stems were chopped into small pieces, dried, and ashed at 400 °C in an open muffle furnace. The batch of *Miscanthus* ash was homogenized in a mortar grinder (Fritsch Pulverisette, type 02.102), and this homogeneous lot was used as a startup sample for further high-temperature experiments. The elemental composition of *Miscanthus* ash samples was determined by scanning electron microscopy–energy-dispersive X-ray analysis (SEM–EDX, Hitachi S4500, FEG, electron beam of 15 kV and resolution of 1 μm^3). The ash samples were carefully mixed and homogenized in a mortar grinder. Then, the ash samples were pelletized and fixed on the sample holder with silver paint. The SEM–EDX analysis was carried out at five different points of the sample, and an average elemental composition was calculated. Table 2 gives the chemical composition of the LM1 (harvested in April) and the LM2 (harvested in September) ash samples. LM2 ash contains significantly higher levels of K and Cl and lower levels of Ca

Table 2. SEM–EDX Analysis (wt %) of LM1 and LM2 Ash Prepared at 400 °C in Air

SEM–EDX analysis of ash samples		
	LM1 at 400 °C (wt %)	LM2 at 400 °C (wt %)
Si	24.2 ± 0.07	13.2 ± 0.10
K	13.7 ± 0.10	33.2 ± 0.20
Ca	11.4 ± 0.08	2.2 ± 0.11
Mg	2.2 ± 0.06	1.2 ± 0.05
Na	0.4 ± 0.04	0.05 ± 0.06
P	0.8 ± 0.04	1.6 ± 0.05
S	1.1 ± 0.04	1.7 ± 0.03
Cl	0.6 ± 0.03	5.0 ± 0.06
Al	0.3 ± 0.03	0.04 ± 0.05
Fe	0.3 ± 0.18	0.0 ± 0.0
O	45.1 ± 0.18	41.9 ± 0.14

DOI: 10.1021/acs.energyfuels.5b01189
Energy Fuels 2015, 29, 6433–6442

than LM1, while the harvest time did not influence the concentration of Mg, P, and S.

2.3. Annealing Tests. The *Miscanthus* ash was studied in an oxidizing atmosphere (air) to describe the inorganic phase transformation under the conditions of combustion. The ash samples were annealed in a laboratory furnace (Nabertherm 30, N7/H, heating rate of 5 °C/min) in the range of 400−1400 °C for 6 h. Approximately 0.4 g of the ash was pressed into a pellet, placed on a Pt−Rh support, and annealed. Then, the samples were quenched in air to freeze the microstructure at a high temperature. The effect of a reducing atmosphere was studied by simulating the gasification conditions around the ash samples in an open laboratory furnace chamber (Inconel 600, d_{int} = 25 mm), located at LTB-Liten (CEA Grenoble, France). The samples were heat-treated at 900 and 1000 °C for 6 h in a reducing gas mixture. The chamber was rinsed with pure N_2 before and after each heat treatment. This device was operated with a total flow rate of 6.15 NL/h, composed of CO_2 (1.8 mol %) and H_2 (3 mol %) gas flows diluted in N_2 because of security regulations. Because of the water-gas shift reaction, the actual composition at 900 and 1000 °C, checked by microgas chromatography, is 0.6 mol % CO_2, 1.8 mol % H_2, 1.2 mol % CO, and 0.2 mol % H_2O. Even though the concentration of the reducing gases is relatively low compared to industrial gasifiers, the partial pressure of oxygen, which has the main effect on inorganic phase transformation,[27] was in the same order of magnitude as during industrial gasification (calculated, $P_{O_2} = 10^{-15}$−10^{-20} bar at 800−1000 °C). Hence, the experiments in a reducing atmosphere are representative to describe the inorganic phase transformation under the conditions of gasification.

2.4. Characterization. The crystalline phases of the ash samples were analyzed by powder X-ray diffraction. The heat-treated ash samples were ground into fine flour consistency. Approximately 0.5 g of ash was placed in the Si sample holder and flattened with a microscopy glass. The diffractograms were recorded on a Bruker D8 Advance diffractometer (cathode Cu Kα1 of 1.5406 Å, 12−70°, detector open at 8°, step at 0.0164°, scan speed of 1 s/scan, 30 kV, 40 mA, division split of 0.7, and rotation of 15 mps). The phase analysis was performed with the software DIFFRACplusEVA using the International Centre for Diffraction Data (ICDD) database.

For the analysis of the molten phase, the heat-treated ash samples were embedded in resin (Epofix Kit, Struers) and polished with water-free lubricants (DP Lubricant Brown and Yellow, Struers). The samples were coated with gold to make them conductive and to improve the imaging.

2.5. Thermodynamic Calculations. *2.5.1. Databases and Solution Phases.* The calculations were performed with FactSage 6.4 software package using FactPS, FToxid, and FTsalt databases. Besides FToxid, another oxide database (GToxid) has been developed by GTT Technology and Jülich Research Center (FZJ) for refractory materials and metallurgical slag.[37] One of the main differences between the two oxide databases is the modeling of the Gibbs energy of the liquid phase. The GToxid liquid phase uses a non-ideal associate model, whereas the FToxid liquid phase uses a quasichemical model. The most important difference for the liquid phase is that the whole alkali domain is attempted to be described by the GToxid database with scarce experimental data available,[29] including many solid Ca−K silicates and solid Mg−K silicates, which are not available in the FToxid database. Table 3 summarizes the databases and liquid solution models used in the calculations.

2.5.2. Input Data. The calculations were performed using the conditions of the laboratory experiments. The input data for 0.4 g of LM1 ash sample is given in Table 4. As the ash was prepared at 400 °C, it still contains unburned carbon. Considering the analysis by SEM−EDX, which can give a rough estimation of the carbon content, 15 wt % of C was added to the elementary composition of LM1 presented in Table 2.

The calculations were performed in both an oxidizing and a reducing atmosphere at atmospheric pressure; the gas inputs for the calculations are presented in Table 5. For an oxidizing atmosphere, there was no air flow in the laboratory furnace. An air volume of 7 L (furnace volume) was estimated to be in equilibrium with the ash sample. For a reducing atmosphere, the quantity of the gas mixture was calculated from the gas flow rate of CO_2 (0.146 L/h) and H_2−N_2 (3 mol % H_2, 6 L/h) for 6 h, which means a total volume of 36.6 L.

Table 3. Databases and Solution Phases Used in the Thermodynamic Equilibrium Calculation

selected liquid and solid solution models		
database	liquid solutions	solid solutions
FactPS		
FToxid	slagA	WOLLA ($CaSiO_3$ and $MgSiO_3$)
		cPyrA ($CaMgSi_2O_6$ and $Mg_2Si_2O_6$)
FTsalt	saltF	ACL_A (solid Cl solution of alkali and alkaline earth metal)
		CSOB (solid alkali sulfate/carbonate solution)
		SCMO (solid binary solution of $MgSO_4$ and $CaSO_4$)
GToxid	LIOX	WOLL ($CaSiO_3$ and $MgSiO_3$)
		CLIN ($CaMgSi_2O_6$ and $Mg_2Si_2O_6$)
		NC2S ($CaSiO_3$ and Na_2SiO_3)

Table 4. Elements Used in the Thermodynamic Calculation (Calculated for a 0.4 g LM1 Ash Sample Prepared at 400 °C in Air)

0.4 g LM1 ash sample	
element	mass (g)
C	0.06
O	0.1516
K	0.0463
Si	0.0809
Ca	0.0398
S	0.0037
Cl	0.0016
Mg	0.0078
P	0.0031
Na	0.0012

Table 5. Gas Input Used in the Thermodynamic Calculations

gas input for calculations	
oxidizing condition	2 g of O_2
	7 g of N_2
reducing condition	1.721 g of CO_2
	0.09642 g of H_2
	43.65 g of N_2

3. RESULTS

3.1. Experimental Results. *3.1.1. Transformation of Solid Phases in an Oxidizing Atmosphere.* Figure 1 represents the transformation of LM1 ash samples as a function of the temperature. Between 400 and 750 °C, the samples look identical, with no major change compared to the startup sample observed. Above 750 °C, the samples stiffen and their color lightens, and around 925−950 °C, they lose the grayish tone. Above 900 °C, because of the volatilization of inorganics, the ash samples blow up, and at 1100−1150 °C, the samples become rounded. Between 1200 and 1250 °C, the amount of liquid phase increases significantly; the ash sample does not keep its shape anymore, and it spreads. A small amount of solid phase is probably still present at 1300−1350 °C, giving the sample an opalescent greenish color. At 1400 °C, the ash

DOI: 10.1021/acs.energyfuels.5b01189
Energy Fuels 2015, 29, 6433−6442

Figure 1. Transformation of LM1 ash sample as a function of the temperature.

sample becomes translucent and is probably completely molten, as confirmed by the XRD characterization.

The diffractograms of samples heat-treated between 400 and 1350 °C are presented in Figure 2. In the range of 400−775 °C,

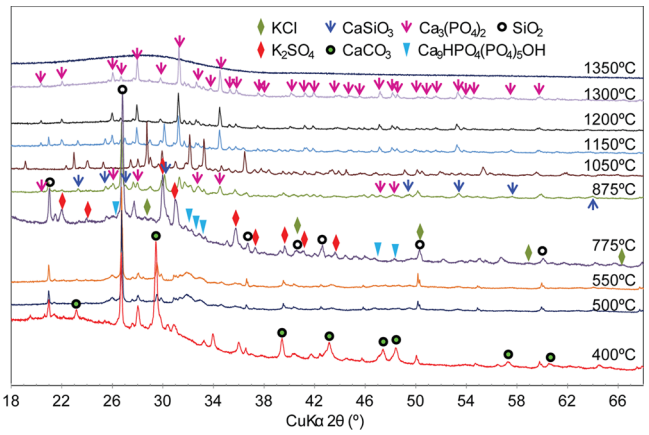

Figure 2. X-ray diffractograms of LM1 ash samples heat-treated in air for 6 h between 400 and 1400 °C.

the main crystalline phases are KCl, K_2SO_4, hydrated Ca phosphate [$Ca_9HPO_4(PO_4)_5OH$], and SiO_2. $CaCO_3$ is present up to 450 °C, and $Ca_9HPO_4(PO_4)_5OH$ becomes detectable around 500−550 °C. A small amount of KCl can be still observed at 775 °C. Around 850−875 °C, the hydrated Ca phosphate transforms into $Ca_3(PO_4)_2$ and a new silicate phase, $CaSiO_3$, appears. Between 1100 and 1150 °C, the peaks of SiO_2 and $CaSiO_3$ gradually decrease, and at 1200 °C, they cannot be detected any more. K_2SO_4 decomposes around 1200−1250 °C, and at 1300 °C, the only solid phase is $Ca_3(PO_4)_2$. At 1350 °C, no crystalline phase can be detected in the diffractograms. It can be noted that no K silicate has been observed at any temperature by XRD.

Figure 3 represents the semi-quantitative analysis of the main crystalline phases using the software EVA. This method is not adequate to quantify the solid phases, but it enables having an idea about the ratio of the different crystalline phases as a function of the temperature. Below 900 °C, the two main crystalline phases are SiO_2 and K_2SO_4 with roughly 40 wt % each. Calcium phosphate is present under different forms with about 10−15%, and KCl was detected in a very small quantity (1−3 wt %) up to 775 °C. Above 900 °C, the main crystalline phase is $Ca_3(PO_4)_2$, representing more than 60 wt %. $CaSiO_3$

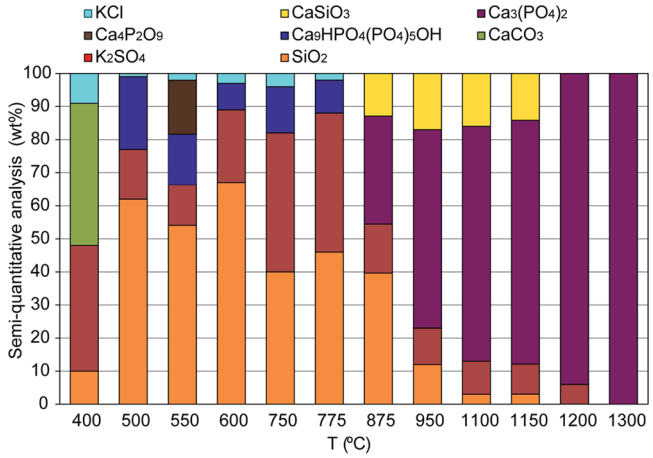

Figure 3. Semi-quantitative analysis of crystalline phases of the LM1 ash sample.

and K_2SO_4 are present up to 1200 °C with about 15 and 10 wt %, respectively.

3.1.2. Effect of the Harvest Period. Figure 4 shows the diffractograms of the LM2 ash sample heat-treated at 400 and

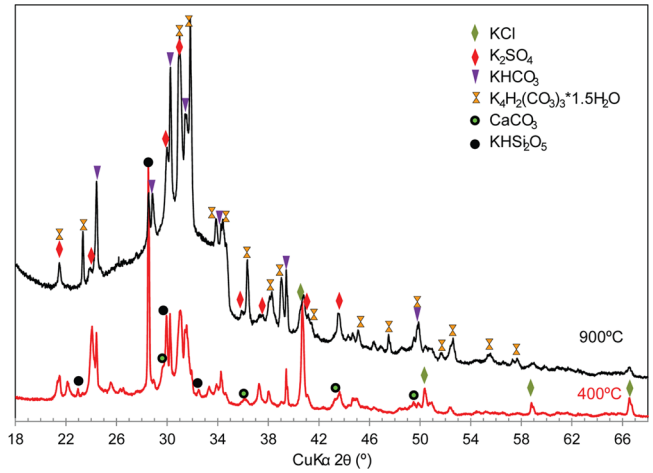

Figure 4. X-ray diffractograms of LM2 ash samples heat-treated for 6 h in air at 400 and 900 °C.

900 °C in air. Because of the elevated amounts of K and Cl and relatively lower amounts of Si and Ca (presented in Table 2), the LM2 ash is mainly composed of K salts (KCl and K_2SO_4), K carbonates [$KHCO_3$, $K_4H_2(CO_3)_3{\cdot}1.5H_2O$, and $CaCO_3$], and K silicate ($KHSi_2O_5$). A very small amount of SiO_2 was also detected in the diffractograms. The main solid compound at 900 °C is $K_4H_2(CO_3)_3{\cdot}1.5H_2O$. It has to be noted that LM2 ash was difficult to manipulate because of the high potassium and lower silica and calcium contents. The ash sample heat-treated at 900 °C was hygroscopic and instable; it changed its color after it was taken out of the furnace and also during recording of the diffractograms. Therefore, it is likely that the carbonates attracted water from the air during the manipulation. Although KCl volatilizes quite easily, a small amount was detected in the LM2 ash sample at 900 °C. It is likely that KCl derives from the deposits on the ash sample surface as a result of the very low air currant in the furnace. It cannot be excluded that diffusion and mass transport limited the KCl release of LM2 ash as a result of its high content in KCl. A longer

DOI: 10.1021/acs.energyfuels.5b01189
Energy Fuels 2015, 29, 6433−6442

annealing duration than 6 h would then be required. At 900 °C, $KHSi_2O_5$ and SiO_2 are molten and only a very small amount of $KHSi_2O_5$ was identified in the diffractograms. No deeper study was performed on these ashes because summer harvest *Miscanthus* is not usually used for gasification or combustion.

3.1.3. Transformation of Solid Phases in a Reducing Atmosphere. Figure 5 shows the X-ray diffractograms of LM1

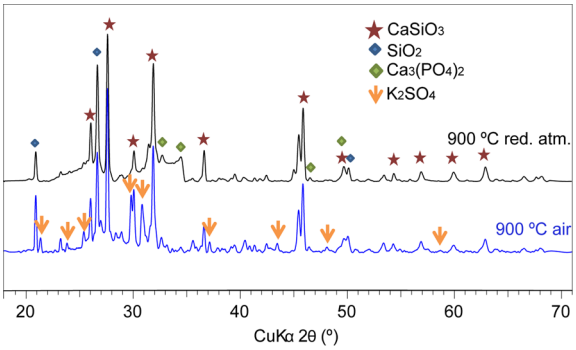

Figure 5. X-ray diffractograms of LM1 ash samples heat-treated in air and in a reducing atmosphere for 6 h at 900 °C.

ashes heat-treated at 900 °C in an oxidizing and a reducing atmosphere. The main difference is the absence of K_2SO_4 under reducing conditions. While S usually forms salts (in most cases, $CaSO_4$ or K_2SO_4) in biomass ashes under oxidizing conditions, it becomes a gaseous compound (mostly H_2S) under reducing conditions. The SEM−EDX analysis showed the presence of unburned organic carbon (not measurable by XRD) with some potassium and sulfur in the molten ashes (Figure 6). Traces of Ca carbonate were also detected by SEM−EDX, but it was not identified by XRD (Figure 6).

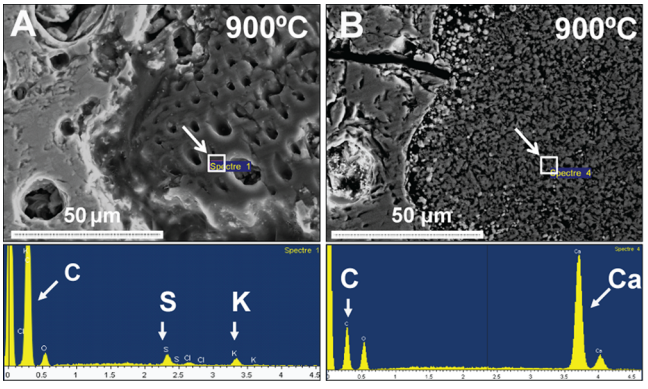

Figure 6. SEM−EDX analysis of LM1 ash samples heat-treated in a reducing atmosphere at 900 °C.

3.1.4. Liquid Phase Composition in Oxidizing and Reducing Atmospheres. Figure 7 shows the composition of molten phases in LM1 and LM2 ash samples heat-treated at 900 °C and analyzed by SEM−EDX. The molten phase is composed of SiO_2, K_2O, and a small amount of CaO and MgO. The composition of the molten ash does not differ significantly between either the oxidizing and reducing atmosphere or between the different harvest periods. No immiscible second liquid phase was observed in any case by SEM−EDX.

3.2. Thermodynamic Calculations. *3.2.1. Evolution of Inorganic Phases at a High Temperature.* The transformation of inorganic phases was described in both oxidizing and

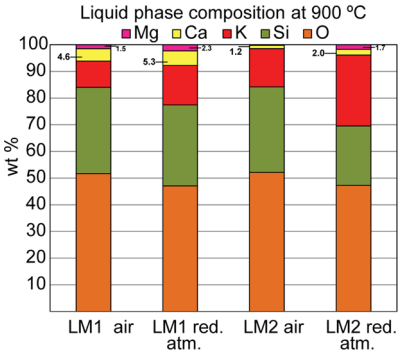

Figure 7. Composition of the molten phase at 900 °C in oxidizing and reducing atmospheres analyzed by SEM−EDX.

reducing atmospheres with two different oxide databases. The evolution of the liquid phase [liquid/solid plus liquid ratio, $L/(L + S) \times 100$] is presented in Figure 8. The ratio of the liquid

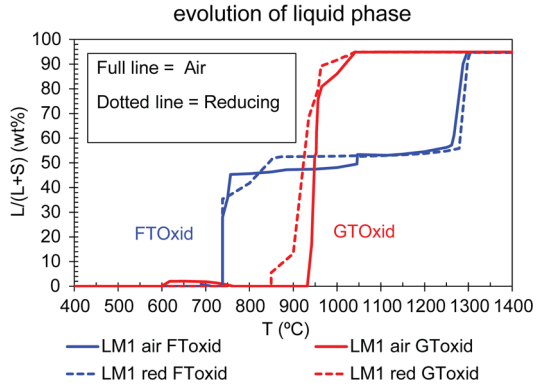

Figure 8. Liquid/liquid plus solid ratio $[L/(L + S) \times 100]$ in LM1 ash as a function of the temperature in air and a reducing atmosphere calculated with FToxid and GToxid databases.

phase significantly differs in the case of the two oxide databases. In the FToxid database, the liquid phase appears at 750 °C and remains around 50 wt % up to 1300 °C. In the GToxid database, the liquid phase appears above 900 °C but rises rapidly above 90 wt %. In both cases, a small difference under oxidizing and reducing conditions can be observed. The inorganic phase transformation of LM1 ash is given in detail in Figures 9 and 10 for the FToxid database and Figures 11 and 12 for the GToxid database.

The difference in the solidus temperature between the two oxide databases is due to the different forms and different melting temperatures of the alkali metal silicates and alkaline earth metal silicates. In FToxid database, K silicates, $CaSiO_3$, and $CaMgS_2O_6$ are formed. The K silicates melt at 750 °C, but the Ca and Mg silicates are in equilibrium with the liquid phase up to 1300 °C, resulting in a relatively lower amount of liquid below 1300 °C. On the other hand, the GToxid database predicts the formation of K−Mg silicates and K−Ca silicates. These silicates are modeled to have a higher melting temperature than K silicates. Hence, the liquid phase appears only around 900 °C (LIOX liquid solution phase). Furthermore, the GToxid liquid phase is modeled to be more stable than the Ca and Mg silicates, which are not any more in equilibrium above 900 °C, contrary to the FToxid database. Hence, there is a higher amount of liquid phase (>90%) with

DOI: 10.1021/acs.energyfuels.5b01189
Energy Fuels 2015, 29, 6433−6442

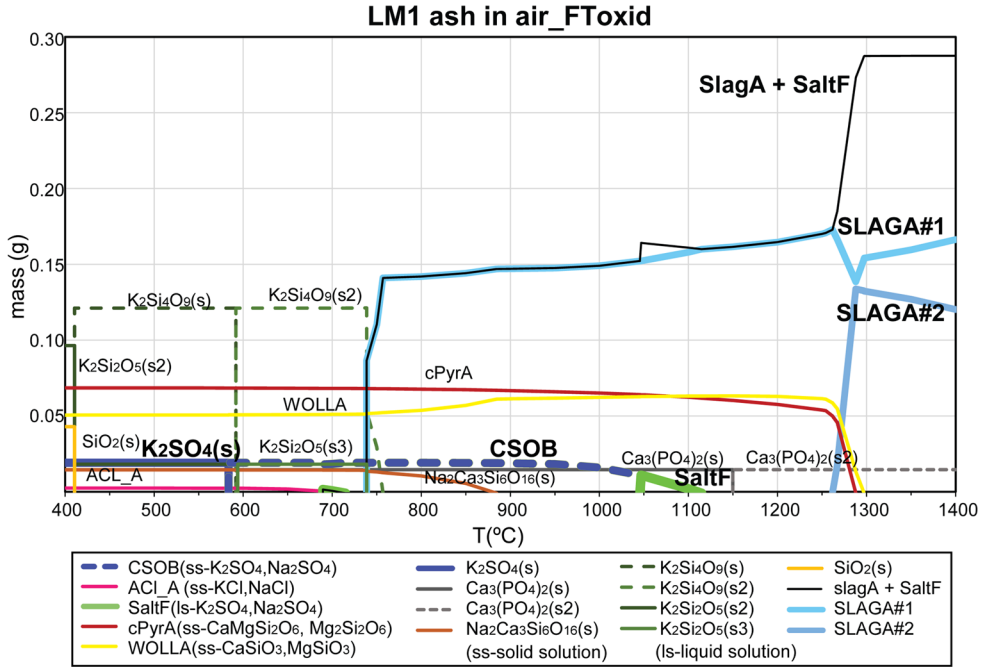

Figure 9. Solid and liquid phases in LM1 ash (air, 1 bar, FToxid−SlagA and FTSalt−SaltF).

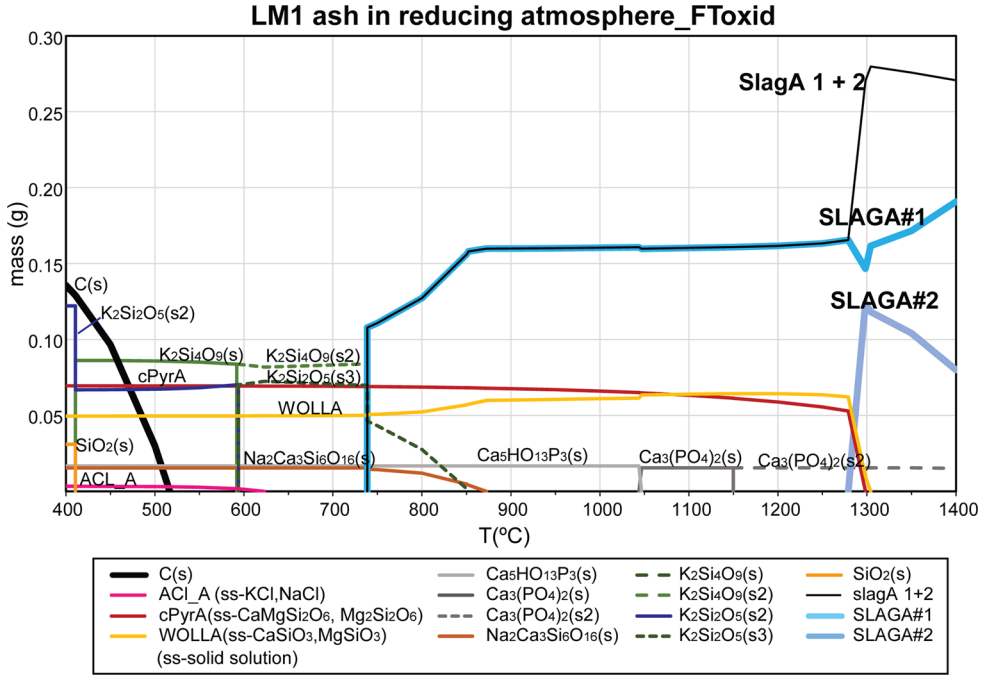

Figure 10. Solid and liquid phases in LM1 ash (reducing atmosphere, 1 bar, FToxid−SlagA and FTSalt−SaltF).

the GToxid database rather than with the FTOxid database above 900 °C.

The difference between oxidizing and reducing atmospheres is due to the form of sulfur. In an oxidizing atmosphere, sulfur is present as solid K_2SO_4 (or CSOB) and it melts (as SaltF) at 1050 °C. In a reducing atmosphere, sulfur is fully released in the gaseous phase as H_2S (g); therefore, more potassium is available to form silicates. Another difference is the form of the phosphorus component in a reducing atmosphere below 1040 °C, which is the hydroxyapatite $Ca_5(PO_4)_3OH$, whereas in an oxidizing atmosphere, it is $Ca_3(PO_4)_2$ in the entire temperature range (400−1400 °C). In any case, SiO_2 is not stable above 450 °C.

4. DISCUSSION/COMPARISON OF EXPERIMENTS AND THERMODYNAMIC MODELING

The experimental investigation and the thermodynamic modeling are compared in Tables 6 and 7. The comparison could be completed in the range of 400−1400 °C for an oxidizing atmosphere (Table 6). In a reducing atmosphere, only few experiments were performed; therefore, the comparison is limited to the compounds present at 900 °C (Table 7).

DOI: 10.1021/acs.energyfuels.5b01189
Energy Fuels 2015, 29, 6433−6442

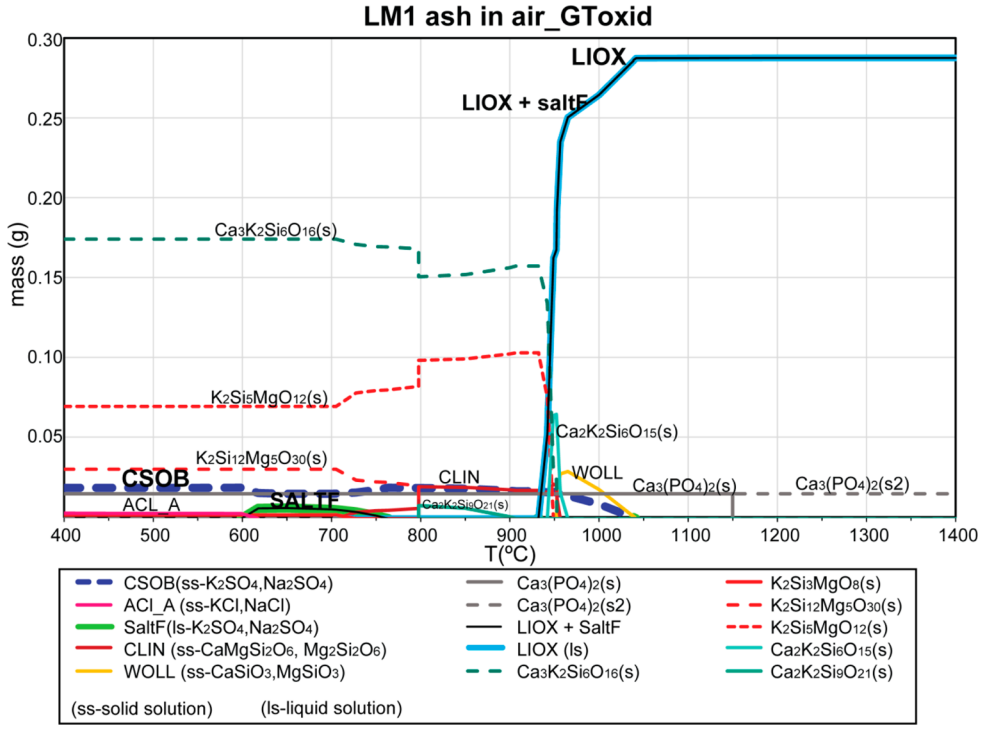

Figure 11. Solid and liquid phases in LM1 ash (air, 1 bar, GToxid−LIOX and FTSalt−SaltF).

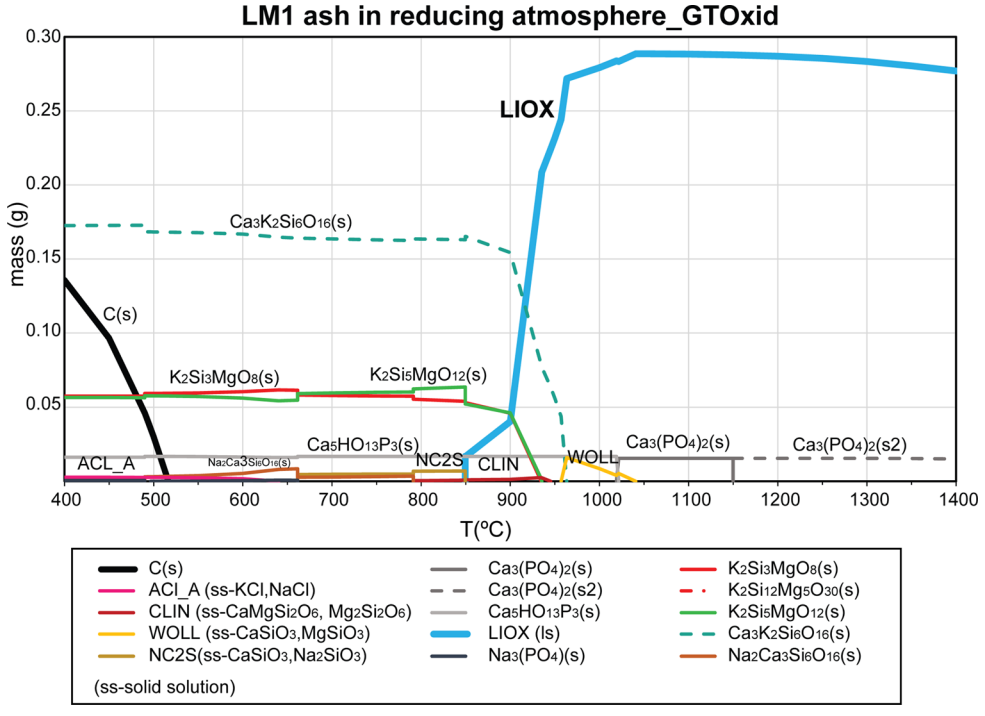

Figure 12. Solid and liquid phases in LM1 ash (reducing atmosphere, 1 bar, GToxid−LIOX and FTSalt−SaltF).

The main solid phases are observed in both calculations and experiments for both atmospheres and thermodynamic databases. The exception is SiO_2, which is not calculated by any databases, and the K−Ca (or Mg) silicates and Ca−Mg silicates, which are not measured with certitude.

In an oxidizing atmosphere, in both FToxid and GToxid databases, the formation of liquid salt solution (SaltF) is possible in a certain temperature range. In the experiments, molten salts or other second molten oxide phases were never detected.

In comparison of Figures 9 and 11 to Figure 3, the trends in the ratio of the quantity of solid phases are described better by the GToxid database than by the FToxid database above 900 °C. In GToxid, the main solid phase is $Ca_3(PO_4)_2$ and the minor phases are K_2SO_4 and $CaSiO_3$. The minor phases decompose between 1000 and 1100 °C. This is very close to the XRD analysis, where $CaSiO_3$ decomposes above 1150 °C

DOI: 10.1021/acs.energyfuels.5b01189
Energy Fuels 2015, 29, 6433−6442

Table 6. Comparing the Detected Temperature Range of the Different Compounds in LM1 Ashes in Experiments and Thermodynamic Calculations in an Oxidizing Atmosphere

LM1 ash in an oxidizing atmosphere			
	experiment	thermodynamic calculation	
compound	XRD, except K silicate (SEM) (°C)	FToxid–Ftsalt (°C)	GToxid–FTsalt (°C)
KCl (s)	400–800	400–600	400–600
K_2SO_4 (s)	400–1200	400–1000	400–1000
$CaCO_3$ (s)	450	–[a]	–
$Ca_3(PO_4)_2$ (s)	500–1300	400–1400	400–1400
SiO_2 (s)	400–1150	400	–
K silicate (s)	600 (SEM)	600–700	–
$CaSiO_3$ (s)	850–1150	400–1200	950–1050
$MgSiO_3$ (s)	?[b]	700–1200	950–1050
$CaMgSi_2O_6$ (s)	?	400–1200	750–950
Mg_2SiO_4 (s)	?	–	600–700
Na–Ca silicate (s)	?	400–900	400–550
Ca–K silicate (s)	?	–	400–950
Mg–K silicate (s)	?	–	400–950

[a]– = not present. [b]? = cannot be detected with certainty.

Table 7. Comparing the Different Compounds in LM1 Ashes in XRD and Thermodynamic Calculations in a Reducing Atmosphere at 900 °C

LM1 (late winter harvest) at 900 °C in a reducing atmosphere			
	experiment	thermodynamic calculation	
compound	XRD	FToxid–FTsalt	GToxid–FTsalt
$Ca_3(PO_4)_2$ (s)	+[a]	–	–
$Ca_5HO_{13}P_3$ (s)	–	+	+
SiO_2 (s)	–	–	–
$CaSiO_3$ (s)	+	+	–
$MgSiO_3$ (s)	?	+	–
$CaMgSi_2O_6$ (s)	?	+	+
Ca–K silicate (s)	+	–	+
Mg–K silicate (s)	?	–	+
$CaCO_3$ (s)	trace[b]	–	–
K_2S and CaS (s)	trace[b]	–	–

[a]+, present; –, not present. [b]Detected by SEM–EDX.

and K_2SO_4 decomposes at 1200 °C. In contrast, FToxid predicts falsely the presence of solid alkaline earth metal silicates up to 1250 and 1300 °C; therefore, it gives a misleading prediction of the quantity of the liquid phase. Unfortunately, it was not possible to quantify the amount of the high-temperature liquid phase by either XRD or SEM to compare to the calculations as a result of the complexity of the ash samples.

In an oxidizing atmosphere, several differences are observed between the experiments and calculations: (1) First, the alkali salts are present up to higher temperatures in laboratory experiments than in the calculations. KCl is still present at 800 °C (versus volatilization above 600 °C in the calculation), and K_2SO_4 is present at 1200 °C (versus 1000 °C). To explain this behavior, it is possible that the volatilized compounds condensed on the surface of the ash sample, because there was no gas flow in the air furnace. It is also possible that the volume taken into account for the calculation was too large, allowing for too high of volatilization of KCl and K_2SO_4. Another explanation is that the sample preparation (pressed in pellets) influenced the volatilization of the salts. (2) The second difference is the absence of alkali metal and alkaline earth metal silicates at low temperatures (<800 °C) in laboratory experiments, whereas these phases are the main solid phases up to the solidus in the calculations regardless of the database and atmosphere. In the X-ray diffractograms, the main solid phase is SiO_2 up to 750 °C and $CaSiO_3$ appears above 800–850 °C, while in the calculations, $CaSiO_3$ (as solid solution WOLLA) and K silicates are already present at 400 °C. The first explanation might be that the *Miscanthus* ash composition is unfortunately located in a boundary of the $CaO–SiO_2–K_2O$ phase diagram,[29] where SiO_2 and wollastonite are not in equilibrium with K silicate or K/Ca (or Mg) silicate or with the melt. The uncertainty of the initial composition measured by SEM, which was used to perform the calculations, might be another cause. Additional calculations were performed with the initial composition of the ash measured at 815 °C (Table 1), which is higher in Si, and results allow for SiO_2 to be present in the calculations. Another cause is the precision of both databases in that area of the phase diagram. For example, the stability (standard enthalpy of formation) of K silicate or K–Ca (or Mg) silicate is not well-known. Furthermore, non-equilibrium phenomena cannot be excluded, because the formation of new mineral phases depends upon the availability and chemical form of the inorganics in the biomass and biomass ash. In the biomass stem, silicon is present as silica gel ($SiO_2 \cdot nH_2O$).[7] In biomass, Ca and Mg are bound to the organic matrix;[1,30] therefore, for the formation of new silicates, first the lignin and cellulose have to decompose. The typical decomposition temperature of cellulose is around 350 °C and around 350–500 °C for lignin. Also, the elements have to be able to reach each other, but often the diffusion of the elements is slower than the chemical reaction itself. The diffusion can be accelerated by the apparition of the liquid phase, which is typically around 750–800 °C for biomass ash. (3) Another difference is the disappearance of Ca phosphate above 1350 °C in the laboratory experiments in air, contrary to the calculation regardless of the database. The XRD measurement showed that, between 1300 and 1350 °C, all of the crystalline phases melt. The complementary SEM–EDX analysis of heat-treated LM1 samples revealed approximately 2 wt % P at 1350 °C and 1 wt % P at 1400 °C in the molten phase.

In a reducing atmosphere at 900 °C, two main differences are observed between the experiments and the calculations: (1) The first one is the presence of unburned organic carbon in the case of LM1 ashes, which can retain other inorganic elements, such as K or S, as proven by the SEM–EDX analysis. The reason for this unburned C is the well-known kinetic limitation of C gasification in the 900 °C temperature range.[38] (2) Another difference concerns the phosphorus phase. Calculations with both databases predict hydroxyapatite $Ca_5(PO_4)_3OH$ to be stable, whereas XRD measurements detect only $Ca_3(PO_4)_2$.

4.1. Composition of the Liquid Phase. Figure 13 compares the equilibrium compositions of liquid phases in LM1 ash at 900 °C obtained by SEM–EDX analysis and GToxid and FToxid databases. In the case of the GToxid database, no liquid phase is present at 900 °C; therefore, the composition predicted at 938 °C is used. FToxid and GToxid use a different approach to describe the liquid phase: in FToxid, the liquid phase is composed of oxides, and in GToxid, the liquid phase is composed of silicates. To be able to compare the

DOI: 10.1021/acs.energyfuels.5b01189
Energy Fuels 2015, 29, 6433–6442

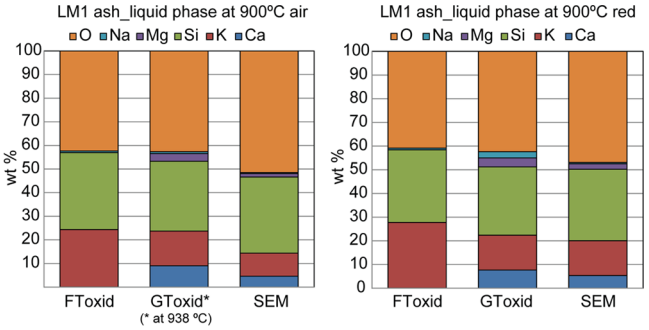

Figure 13. Comparison of liquid phase composition of LM1 ash at 900 °C between FToxid–slagA and GToxid–LIOX databases and SEM–EDX measurements.

SEM analysis to the different databases, the elemental compositions were calculated for each case.

The FToxid database predicts two main components, K_2O and SiO_2, and a very small quantity of Na_2O (<1 wt %). The liquid oxide solution in GToxid contains Mg and Ca as well, which gives a better description of the experimentally observed composition.

Although the composition of the liquid phase is better described with GToxid, the apparition of the liquid phase (938 °C for an oxidizing atmosphere and 900 °C for a reducing atmosphere) is considered to be too high compared to the experimental observations. The exact temperature of liquid phase appearance could not be determined exactly with experiments, although previous differential scanning calorimetry (DSC) analysis[39] and visual observation indicates that the ash sample starts to melt around 750–775 °C.

5. CONCLUSION

The XRD analysis of the *Miscanthus* ash revealed the complex phase transformations as a function of the temperature. At moderate temperatures (<750 °C), most of the inorganics form salts [KCl, K_2SO_4, and $Ca_3(PO_4)_2$], carbonates, and silica. With increasing the temperature, the formation of alkaline earth metal silicates is favored. Above 1000 °C, the crystalline phase declines and the ash completely melts between 1300 and 1350 °C. It was found that the harvest period can significantly modify the composition of *Miscanthus* ash. *Miscanthus* harvested at the end of summer (LM2) contains almost 3 times more potassium and 5 times less calcium as the spring harvest (LM1), resulting in the presence of potassium carbonates and silicates at both 400 and 900 °C.

The main difference between oxidizing and reducing atmospheres is the form of sulfur. In an oxidizing atmosphere, sulfur forms K_2SO_4, while in a reducing atmosphere, only some organically attached S was detected by SEM–EDX analysis. Unburned carbon is also observed in a reducing atmosphere.

The experiments were compared to thermodynamic calculations using the software package FactSage. Two different oxide databases, FToxid or GToxid, were compared to the experiments performed under equilibrium conditions. The GToxid database predicts a higher solidus temperature (T_s > 900 °C) but greater liquid/solid ratio. Both databases predict the formation of K silicates or K–Ca (Mg) silicates below 800 °C, while the main solid phase observed by XRD was SiO_2. Reasons are linked to uncertainties in the initial mass balance of ashes, database uncertainties, and limitations of the diffusion and chemical reaction of elements, which are organically bound to the biomass structure, as revealed by many studies.[1,40] On the other hand, GToxid describes the trends of the main solid phases as a function of the temperature better than FToxid above 950 °C. The composition of the liquid phase is well-described in both databases, although GToxid gives somewhat closer results to the SEM–EDX analysis with the incorporation of Ca and Mg into the liquid phase.

These differences indicate that, for the moment, no universal database is available to describe the phase transformation of biomass ashes at a high temperature. Equilibrium calculations can be used to estimate the biomass ash melting behavior and as a complementary tool to interpret the experiments, but these results have to be handled with care because the calculations have certain limits.

AUTHOR INFORMATION

Corresponding Author

*E-mail: kaknicsjudit@gmail.com.

Notes

The authors declare no competing financial interest.

ACKNOWLEDGMENTS

NovaBiom is acknowledged for the supply of *Miscanthus*. The authors gratefully acknowledge Emmanuel Véron for his help with the XRD analysis. Special acknowledgement is extended to Annie Richard and Marie-Laure Bouchetou for the SEM–EDX analyses.

REFERENCES

(1) Andrea Jordan, C.; Akay, G. *Fuel* **2012**, *91*, 253–263.
(2) Zhang, Y.; Ashizawa, M.; Kajitani, S.; Miura, K. *Fuel* **2008**, *87*, 475–481.
(3) Dupont, C.; Nocquet, T.; Da Costa, J. A.; Verne-Tournon, C. *Bioresour. Technol.* **2011**, *102*, 9743–9748.
(4) Lewandowski, I.; Clifton-Brown, J. C.; Scurlock, J. M. O.; Huisman, W. *Biomass Bioenergy* **2000**, *19*, 209–227.
(5) Werkelin, J.; Skrifvars, B.-J.; Zevenhoven, M.; Holmbom, B.; Hupa, M. *Fuel* **2010**, *89*, 481–493.
(6) Bryers, R. W. *Prog. Energy Combust. Sci.* **1996**, *22*, 29–120.
(7) Ma, J. F.; Yamaji, N. *Trends Plant Sci.* **2006**, *11*, 392–397.
(8) Vassilev, S. V.; Baxter, D.; Andersen, L. K.; Vassileva, C. G. *Fuel* **2013**, *105*, 40–76.
(9) Boström, D.; Skoglund, N.; Grimm, A.; Boman, C.; Ohman, M.; Brostrom, M.; Backman, R. *Energy Fuels* **2012**, *26*, 85–93.
(10) Bartels, M.; Lin, W.; Nijenhuis, J.; Kapteijn, F.; van Ommen, J. R. *Prog. Energy Combust. Sci.* **2008**, *34*, 633–666.
(11) Vassilev, S. V.; Baxter, D.; Vassileva, C. G. *Fuel* **2014**, *117*, 152–183.
(12) Dupont, C.; Rougé, S.; Berthelot, A.; Da Silva Perez, D.; Graffin, A.; Labalette, F.; Laboubée, C.; Mithouard, J.-C.; Pitocchi, S. *Int. J. Chem. React. Eng.* **2010**, DOI: 10.2202/1542-6580.1949.
(13) Visser, H. J. M. *The Influence of Fuel Composition on Agglomeration Behaviour in Fluidised-Bed Combustion*; Energy Research Centre of the Netherlands (ECN): Petten, Netherlands, Sept 2004; ECN-C--04-054.
(14) Vamvuka, D.; Zografos, D. *Fuel* **2004**, *83*, 2051–2057.
(15) Jenkins, B. M.; Baxter, L. L.; Miles, T. R. J.; Miles, T. R. *Fuel Process. Technol.* **1998**, *54*, 17–46.
(16) Mac an Bhaird, S. T.; Walsh, E.; Hemmingway, P.; Maglinao, A. L.; Capareda, S. C.; McDonnell, K. P. *Powder Technol.* **2014**, *254*, 448–459.
(17) Kupka, T.; Mancini, M.; Irmer, M.; Weber, R. *Fuel* **2008**, *87*, 2824–2837.
(18) Sommersacher, P.; Brunner, T.; Obernberger, I. *Energy Fuels* **2012**, *26*, 380–390.

DOI: 10.1021/acs.energyfuels.5b01189
Energy Fuels 2015, 29, 6433–6442

(19) Lindberg, D.; Backman, R.; Chartrand, P.; Hupa, M. *Fuel Process. Technol.* **2013**, *105*, 129−141.
(20) Berjonneau, J.; Colombel, L.; Poirier, J.; Pichavant, M.; Defoort, F.; Seiler, J.-M. *Energy Fuels* **2009**, *23*, 6231−6241.
(21) Froment, K.; Defoort, F.; Bertrand, C.; Seiler, J. M.; Berjonneau, J.; Poirier, J. *Fuel* **2013**, *107*, 269−281.
(22) Evic, N.; Brunner, T.; Obernberger, I. *Proceedings of the 20th European Biomass Conference and Exhibition*; Milan, Italy, June 18−22, 2012.
(23) Li, H.; Yoshihiko, N.; Dong, Z.; Zhang, M. *Chin. J. Chem. Eng.* **2006**, *14*, 784−789.
(24) Van Dyk, J. C.; Melzer, S.; Sobiecki, a. *Miner. Eng.* **2006**, *19*, 1126−1135.
(25) Elled, A.; Åmand, L.; Steenari, B. *Fuel* **2013**, *111*, 696−708.
(26) Grimm, A.; Öhman, M.; Lindberg, T.; Fredriksson, A.; Boström, D. *Energy Fuels* **2012**, *26*, 4550−4559.
(27) Petit, M.; Froment, K.; Patisson, F.; Seiler, J.-M.; Defoort, F. *Proceedings of the 17th European Biomass Conference and Exhibition*; Hamburg, Germany, June 29−July 3, 2009.
(28) *FactSage Database Documentation*; http://www.crct.polymtl.ca/fact/documentation/.
(29) Levin, E. M.; Robbins, C. R.; McMurdie, H. F. *Phase Diagrams for Ceramists*; Reser, M. K., Ed.; The American Ceramic Society: Westerville, OH, 1964.
(30) Zevenhoven-Onderwater, M.; Backman, R.; Skrifvars, B.; Hupa, M. *Fuel* **2001**, *80*, 1489−1502.
(31) Vassilev, S. V.; Baxter, D.; Andersen, L. K.; Vassileva, C. G. *Fuel* **2013**, *105*, 19−39.
(32) Vassilev, S. V.; Baxter, D.; Andersen, L. K.; Vassileva, C. G.; Morgan, T. J. *Fuel* **2012**, *94*, 1−33.
(33) Rizvi, T.; Xing, P.; Pourkashanian, M.; Darvell, L. I.; Jones, J. M.; Nimmo, W. *Fuel* **2015**, *141*, 275−284.
(34) Baxter, X. C.; Darvell, L. I.; Jones, J. M.; Barraclough, T.; Yates, N. E.; Shield, I. *Fuel* **2012**, *95*, 50−62.
(35) Kaknics, J.; Michel, R.; Richard, A.; Poirier, J. *Energy Fuels* **2015**, *29*, 1785−1792.
(36) Osman, E. A.; Goss, J. R. *Am. Soc. Agric. Eng.* **1983**, *83*, 3549−3565.
(37) Hack, K.; Jantzen, T.; Müller, M.; Yazhenskikh, E.; Wu, G. *Proceedings of the 5th International Congress on the Science and Technology of Steelmaking*; Dresden, Germany, Oct 1−3, 2012.
(38) Kersten, S. R. A.; Prins, W.; van der Drift, A.; Swaaij, W. *Proceedings of the 12th European Conference on Biomass for Energy, Industry and Climate Protection*; Amsterdam, Netherlands, June 17−21, 2002; Vol. *1*, pp 556−559.
(39) Michel, R.; Kaknics, J.; Bouchetou, M. L.; Gratuze, B.; Balland, M.; Hubert, J.; Poirier, J. *Chem. Eng. J.* **2012**, *207*−*208*, 497−503.
(40) Pettersson, A.; Zevenhoven, M.; Steenari, B.-M.; Åmand, L.-E. *Fuel* **2008**, *87*, 3183−3193.

DOI: 10.1021/acs.energyfuels.5b01189
Energy Fuels 2015, 29, 6433−6442